Academic International Journal of Engineering Science
ISSN: 2984-7745
Aca. Intl. J. E. Sci. 2026; 4(1) 24-42
Journal homepage: www.aipublishers.org/aijes

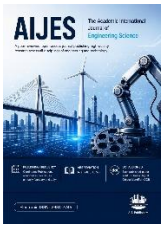

Finite Element Study on Flexural Behaviour of Wide Concrete–Cellular Steel Composite Beams

Raid A. Daud[1], Al-Mortadha O. ABED[2], Mustafa H. Al-Allaf[3], Fahed Alrshoudi[4] and Sultan A. Daud[5]*

[1]Assistant Professor, Dept. of Forensic Eng., Higher Institute of Forensic Sciences, Al-Nahrain University, Baghdad-Iraq.
raid.a.daud@nahrainuniv.edu.iq
[2]MSc Graduate, Civil Engineering Department, College of Engineering, Al-Nahrain University, Baghdad, Iraq
[3]Doctor, Civil Engineering Department, College of Engineering, Al-Nahrain University, Baghdad, Iraq.
[4]Associate Professor, Civil Engineering Department, King Saud University, Riyadh11421, Suadi Arabi.
falrshoudi@ksu.edu.sa
[5]Assistant Professor, Civil Engineering Department, College of Engineering, Al-Nahrain University, Baghdad, Iraq.
sultan.a.daud@nahrainuniv.edu.iq
*. Correspondence: sultan.a.daud@nahrainuniv.edu.iq

Article Info.
Article history:
Received 2 December 2025
Revised 18 December 2025
Accepted 2 February 2026
Published 17 February 2026
Keywords:
FE analysis; composite beams; steel–concrete interaction; shear connectors; cellular steel beams; opening shapes.
How to cite:
Raid A. Daud, Al-Mortadha O. ABED, Mustafa H. Al-Allaf, Fahed Alrshoudi, Sultan A. Daud. Finite Element Study on Flexural Behaviour of Wide Concrete–Cellular Steel Composite Beams. Aca. Intl. J. E. Sci. 2026;4(1) 24-42.
DOI:
https://doi.org/10.59675/E412

Abstract

Wide concrete–cellular steel composite beams have emerged as an efficient structural solution for achieving enhanced the flexural behaviour, reducing self-weight, and improving the long-term behaviour in modern construction. This paper aims to investigate the flexural behaviour of composite wide concrete/cellular beams using nonlinear finite element compactional package ABAQUS 6.19. An experimental date from Victoire et al. (2024) was employed to build the numerical model. Load-deflection, load-slip and the modes of failure were the main parameters that investigated to check the accuracy of the numerical model. Extensive parametric studies using the validated model were conducted to understand the effects of varying opening shape, opening number, and connector configuration on flexural behaviour. The numerical results indicate that optimizing opening shapes, numbers and connector configuration leads to a desirable balance between stiffness, strength, and ductility. Based on the numerical work conducted, it was found that circular and octagonal openings exhibited superior load-carrying capacity and ductility performance compared to those with rectangular or square openings, which suffered from high stress concentrations.

1. Introduction

The dominated use of steel/concrete composite systems as modern infrastructure is owing to their capability to merge the tensile resistance of steel with the compressive strength of concrete into a single

high-performance unit. Additionally, this connection allows composite structures such as bridges and multi-story buildings to satisfy the required strength and stiffness for any desired application [1-3].Although composite structures, in terms of fundamental understanding and characterization composite action behaviour, has reached an advanced stage, the use of mechanical shear connectors are still requiring further research, in particular understanding the nonlinear composite behaviour (i.e. reduced deflections, enhanced ductility, and delayed collapse modes) of the different connecter configuration. This is vital for appropriate design of Concrete-Cellular Steel (CCS) composite beams [4-7]. The nonlinear composite behaviour is influenced by several parameters such as configuration and mechanical properties of shear connectors, furthermore, steel web geometry and the concrete part thickness. Headed stud connectors are usually preferred in connection between the steel beam and concrete slab due to their strong mechanical interlock; However, the connectors remain embedded within the concrete part, sophisticating the structural reconstruction process and making their dismantling impossible [8-13].

Several studies were proposed different such as blind-bolted connectors, locking-nut systems, and long tubular connectors that distribute stresses over greater concrete areas to reduce localized crushing and enhance workability during different loading conditions. It was previously showed that, bolted connectors offered better slip capacity than welded connectors which in turns improve durability [14-16]. Despite this progress, the practical application of some alternative connector techniques still needs specialized tools, resulting in reduced construction efficiency and limited adoption.

Also, numerical and theoretical research proved that, concentrating shear studs near supports improve the overall behaviour due to the high shear forces in those areas. However, poor interaction leads to increased deformation and premature failures caused by relative slip. Illustrating that, partially connected composite beams remain the weakest structural member if not designed carefully [17-22].

In recent years, steel design was proposed toward more complex composite sections, aiming to reduce self-weight together with enhancing structural capacity. Wide CCS beams represent one such innovative type, where openings are created to the steel webs to reduce material usage and facilitate service integration. Concurrently, opening introduces stress redistribution effects. This phenomenon must be carefully evaluated to ensure safe design performance [23-25].

Finite Element Analysis (FEA) has considered as an essential computational tool to understand the structural behaviour of these composite beams type i.e. CCS. ABAQUS is widely used for its ability to simulate the nonlinear behaviour for both steel and concrete. In particular, concrete cracking and crushing, steel plasticity, and contact interaction at the interface making it ideal for evaluating composite beam flexural behaviour under different loading conditions.

Despite extensive research on composite beams and shear connectors. A significant research gap still existed regarding the flexural behaviour and interaction of wide CCS beams. The unique geometry of cellular steel sections presents a complex behaviour, necessitating a systematic understanding of stress transfer across the cellular steel web section and the concrete section, as well as the role of shear stud configuration in maintaining the composite mechanisms while resisting slip at the interface. Furthermore, the presence of opening and the reduced web area influence the initiation of plastic hinges and the web susceptibility to local instability including web post buckling, during bending.

Therefore, this research aims to investigate the flexural behaviour of wide CCS beams using nonlinear FE software. Particularly focusing on evaluating the load and deflection characteristics, failure

Aca. Intl. J. E. Sci. 2026;4(1) 24-42. **DOI***:* https://doi.org/10.59675/E412

mechanisms, internal stress distribution and the efficiency of shear force transmission across the steel/concrete interface.

2. Summary of the Experimental Study Used for Validation

Victoria et al. (2024) [26] conducted an experimental study to examine the bending behaviour and composite interaction between RC slabs and steel beams. The test specimens consisted of steel beams covered with RC slabs and mechanically connected via shear studs to provide partial or complete interaction. The properties of both the steel and RC were assessed prior to testing to ensure their accurate representation in the structural analysis.

The composite beams were simply supported and subjected to monotonous loading using a four-point loads (see Figure 1). This experimental setup allowed monitoring flexural cracking and crushing in the RC slab. Linear variable displacement transducers (LVDTs) were attached at the mid-span and supports to monitor vertical deflection throughout the loading sequence.

These instrumentations, conducted by Victoire, 2024 [26], were used as a reference database to validate the FE models developed in this study. By comparing the observed structural responses, such as load deflection behaviour, and failure patterns, with the corresponding numerical findings, the reliability of the numerical modeling were confirmed.

2.1 FE Model Geometry and Material Properties

To accurately investigate numerically the flexural behaviour of composite beams observed in the experimental reference study (Victoire et al., 2024) [26], a detailed three-dimensional FE model was developed (see Figure 1) using ABAQUS version 6.19. The composite beams span length was 2500mm and subjected to a four-point loading configuration applied symmetrically about the mid-span.

The RC slab measured 405 mm in width and 90 mm in thickness as illustrated in Figure (1). The slab was reinforced with 8 mm diameter steel bars arranged in both longitudinal and transverse directions at 115 mm spacing, in line with conventional reinforcement detailing practices for composite slabs. The steel beam section had chosen an IPE AA 140 profile. The mechanical shear connectors were numerically created as headed studs with 13 mm diameter and 60 mm height positioned in a single row along the top flange. In the fully composite beam configuration (CBFS), a total of twenty-eight headed studs were arranged at 90 mm intervals (see Figure 2 (a)). A partially composite configuration (CBPS) was also numerically represented by reducing the number of studs to fourteen (See Figure 2(b, c, and d)), an approximate 50% degree of shear connection.

In the FE simulation, the steel beam was modeled using 8-node linear brick elements with reduced integration (C3D8R), and exhibited as elastic- plastic material with strain hardening. The RC slab part was also modeled using same above solid elements (C3D8R), enabling to capture three-dimensional elastic and plastic stresses, within cracking and crushing concrete regions (adopting Concrete Damage Plasticity (CDP) material model). Reinforcement steel bars were represented as 2-node truss elements (T3D2) inserted within the RC slab part using the “embedded region”. Steel reinforcement materiel was also modeled using same above steel beam material representation. The mechanical shear connectors were simulated using solid elements (C3D8R). For improve accuracy of the numerical model in evaluating partial interaction effects, cohesive surface approach was also introduced in present numerical analyses. Applied line uniform loading and boundary conditions were simulated using solid elements (C3D8R) as steel bearing plates to uniformly distribute applied loads and reactions.

Aca. Intl. J. E. Sci. 2026;4(1) 24-42. **DOI**: https://doi.org/10.59675/E412

The material properties used in the FE model were adopted from the experimental study conducted by Victoire et al. (2024) [26]. The average compressive strength (fcu) was varied from 25.3 to 27.0 MPa the splitting tensile strength was ranged between 2.5 and 2.7 MPa. Reinforcement in the RC slab consisted of D8 high-yield deformed bars with a yield strength of 437.7 MPa, an ultimate tensile strength of 561.9 MPa.

The steel beam was fabricated using an IPE AA 140 section of S355 grade structural steel. The material exhibited a yield strength of 387.1 MPa, an ultimate tensile strength of 538.8 MPa. The shear connection between the steel beam and the RC slab was achieved through headed shear studs made of mild steel. The yield strength of the studs was 339 MPa, whereas the ultimate strength was 456 MPa.

Aca. Intl. J. E. Sci. 2026;4(1) 24-42. **DOI***:* https://doi.org/10.59675/E412

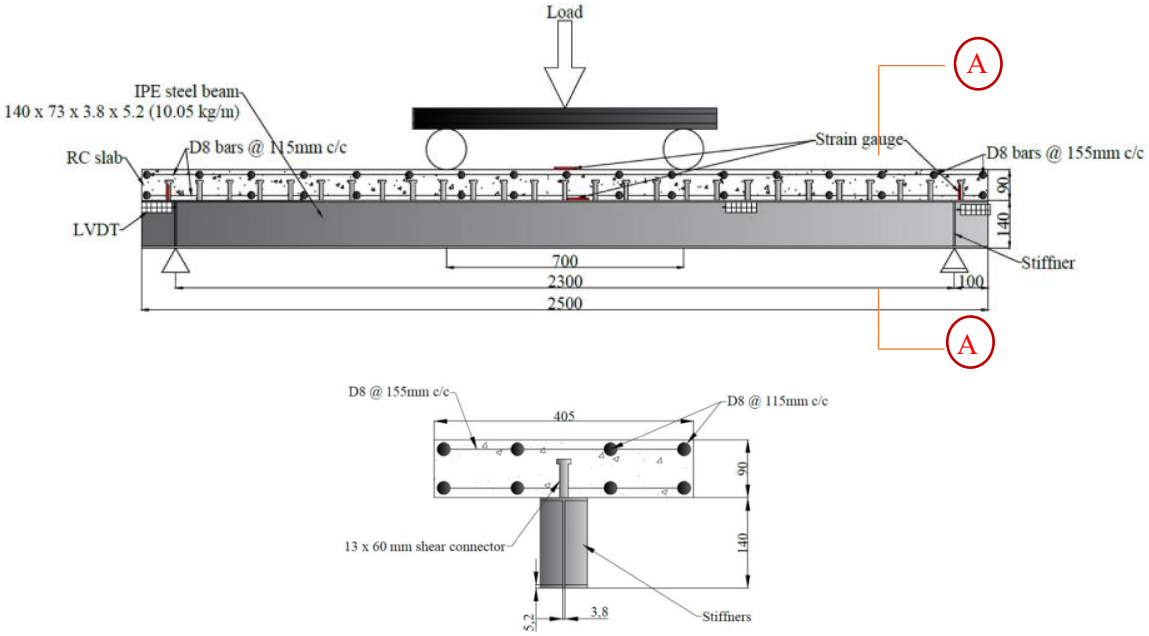

Section A-A

(a)

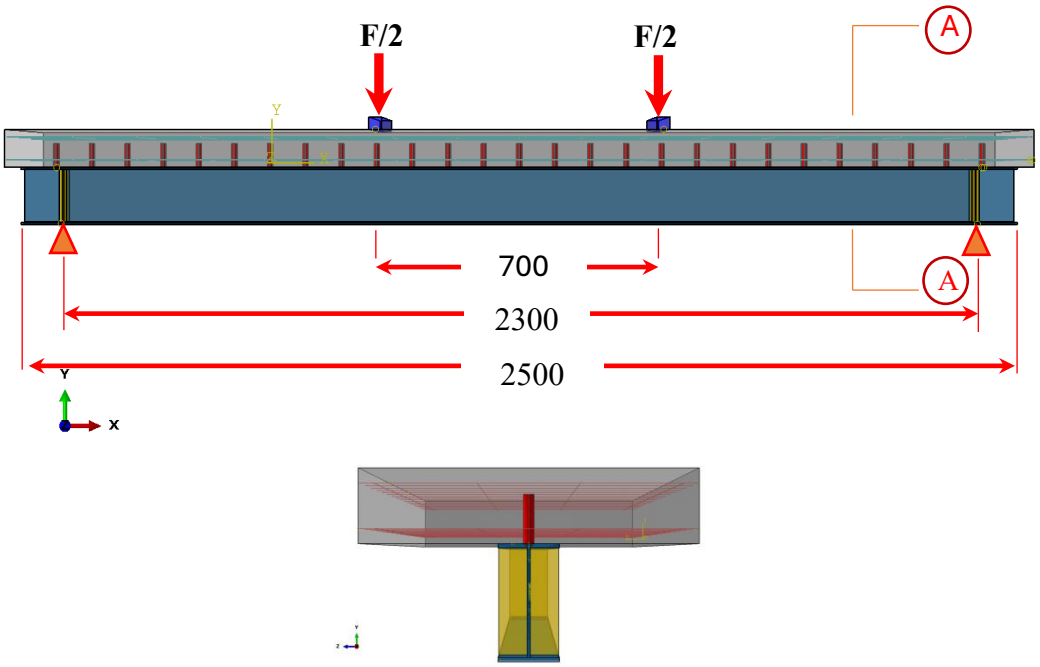

Section A-A

(b)

Figure 1. Composite Beam Test Setup (a) Experimental (b) Numerical model

Aca. Intl. J. E. Sci. 2026;4(1) 24-42. **DOI**: https://doi.org/10.59675/E412

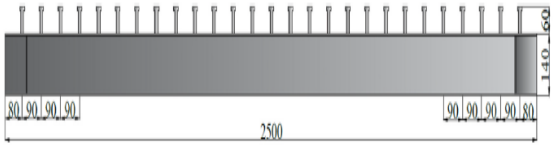

I- Experimental

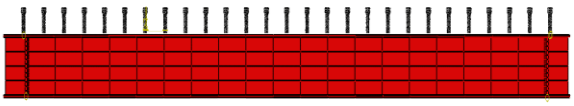

II- Numerical

(a) Beam with Full Shear Connection (Uniform Distribution of

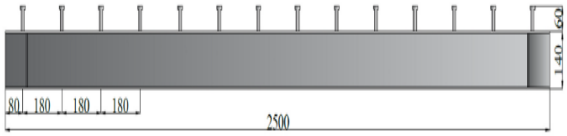

I- Experimental

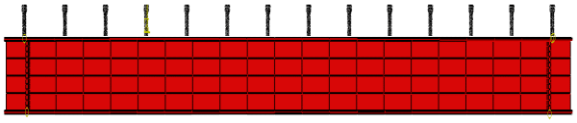

II- Numerical

(b) Beam with Partial Shear Connection (Uniform Distribution of

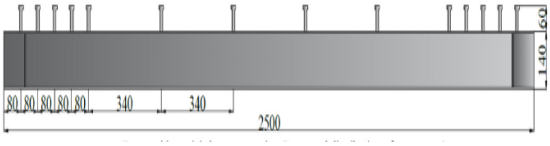

I- Experimental

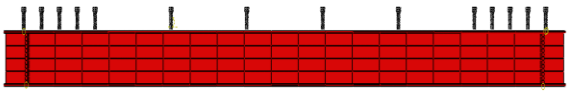

II- Numerical

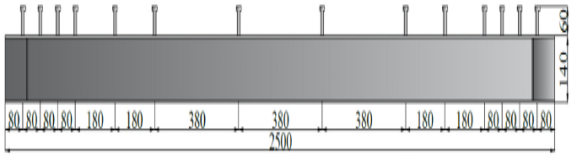

I- Experimental

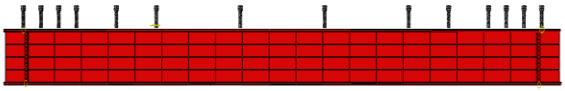

II- Numerical

Figure 2. Different layout of The Shear Stud Connectors

Aca. Intl. J. E. Sci. 2026;4(1) 24-42. **DOI**: https://doi.org/10.59675/E412

3. Validation Results

The accuracy of the developed FE model was assessed by comparing experimental findings reported by Victoire et al. (2024) [26] with that predicted by the FE model. Four samples were used to validate the numerical model. This validation was focused on key parameters i.e. load–deflection, ultimate load capacity, stiffness, and failure modes. The close agreement between numerical and experimental outcomes confirmed the validity of the adopted FE model.

3.1. Load–Deflection Relationships

The comparison of load–deflection curves between experimental and numerical results (Figure 3) demonstrates excellent correlation across all beam configurations. Both datasets exhibit an initial linear response corresponding to the elastic phase, followed by a nonlinear region governed by the onset of cracking in the RC slab and yielding in the steel beam.

For the fully composite beam (CBFS), the FE model accurately reproduced the stiffness and post-yield ductility observed experimentally. The predicted ultimate load was within 5% of the test results, validating the constitutive material models and load-application approach.

In the partially connected beam (CBPS) and stepped configurations, the FE results also followed the same nonlinear trend as the experimental curves. Slight overestimation of mid-span deflection at high load levels was observed (within percentage error 8 %), likely due to the simplified representation of concrete cracking and localized crushing near the loading zones. Nonetheless, the general agreement across all stages of loading demonstrates the model's robustness in predicting the flexural response and the degradation of stiffness leading up to failure.

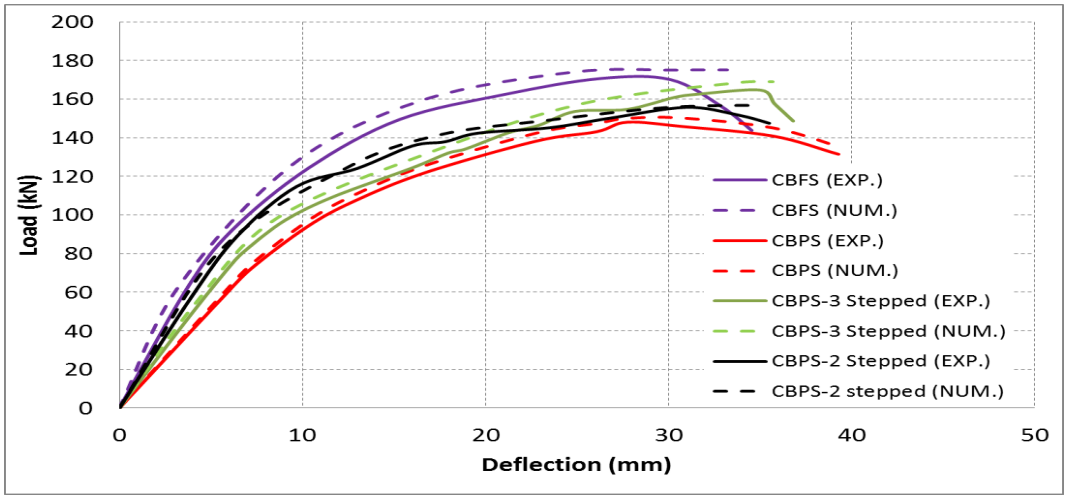

Figure 3. Validations Load-Deflection Curves of Composite Beams.

Aca. Intl. J. E. Sci. 2026;4(1) 24-42. **DOI**: https://doi.org/10.59675/E412

3.2 Failure Modes

The experimental and numerical failure patterns of all beam configurations are illustrated in Figures (4–7). Overall, the FE (FE) analysis successfully reproduced the sequence, distribution, and type of failures observed in the laboratory tests.

In case of CBFS, both experimental and numerical results exhibited a typical flexural failure mode governed by the interaction of tensile cracking in the RC slab, compressive crushing at the loading points, and yielding of the steel section in mid-span zone. In the FE results, both stress and strain contours (as shown in Figure 4b), showed high compressive stresses concentrated at the upper concrete surface beneath the loading points accompanied by maximum tensile stresses along the slab. At ultimate load, localized RC crushing developed in the compression zone. Whereas steel beam exhibited plastic deformation in the bottom flange, forming plastic hinge. This failure pattern agrees closely with the experimental observations.

In the second case i.e. CBPS, the FE model revealed a more complex failure process characterized by progressive interfacial slip and earlier crack initiation compared to the fully composite specimen. Due to the reduced number of shear connectors, shear transfer across the interface was partially compromised. This led to a localized stress concentration around the connectors and along the steel flange (see Figure 5). The good agreement between the experimental and numerical findings verification that the FE model effectively captured the influence of reduced shear connection on the overall load transfer mechanism and flexural behaviour.

For the 2-stepped and 3-stepped connector (Figure 6 and Figure 7) configurations, both the experimental and numerical finding demonstrated significantly enhanced behaviour compared to the uniformly distributed partial connection. The FE model showed that, the stepped connector layout promoted a more uniform shear stress distribution along the beam/slab interface. As a result, failure occurred in more distributed and ductile manner. Cracks in the RC slab were finer and more evenly spread along the span which, in turn resulted in less localized RC crushing.

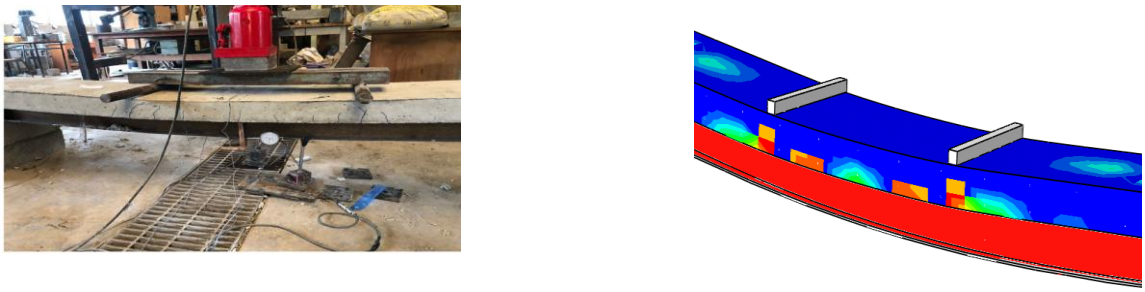

(a) (b)

Figure 4. Validations Failure Modes of Composite Beam CBFS (a) Experimental (b) Numerical

Aca. Intl. J. E. Sci. 2026;4(1) 24-42. **DOI**: https://doi.org/10.59675/E412

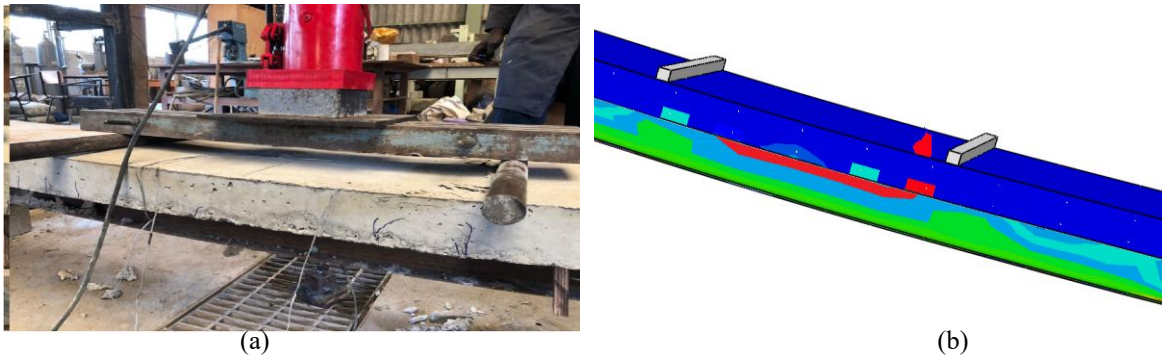

(a) (b)

Figure 5. Validations Failure Modes of Composite Beams CBPS (a) Experimental (b) Numerical

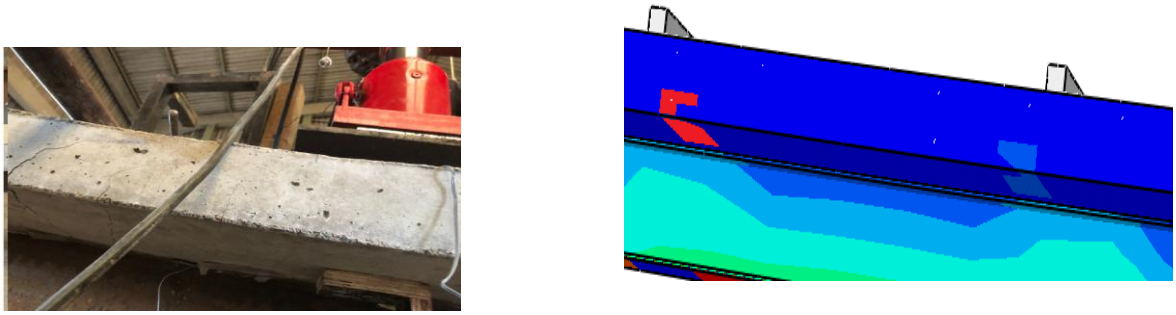

(a) (b)

Figure 6. Validations Failure Modes of Composite Beam CBPS-2-stepped (a) Experimental (b) Numerical

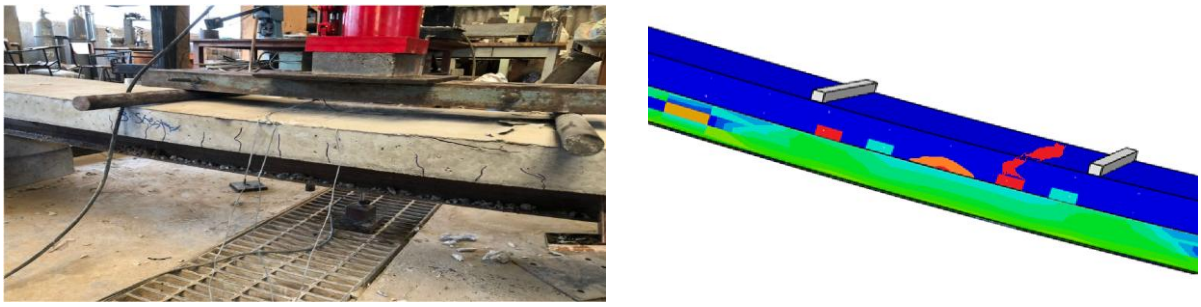

(a) (b)

Figure 7. Validations Failure Modes of Composite Beams CBPS-3-stepped (a) Experimental (b) Numerical

Aca. Intl. J. E. Sci. 2026;4(1) 24-42. **DOI**: https://doi.org/10.59675/E412

4. Key Parameters Discussion

The FE simulations of wide CCS composite beams revealed systematic trends in flexural performance, stiffness, ductility, and failure mechanisms. All of which were significantly influenced by the geometry of the web openings, the number of openings, and the degree of shear connection (η) between the steel beam and the RC wide beam.

Table 1 showed the ultimate load capacity (Fu) from the FE analysis. It can be seen that Fu was clearly dependent on both opening geometry and composite interaction level. In Case 1, i.e. CBFS, ultimate loads ranging from 125 kN to 166 kN were exhibited by the fully composite beams. Whereas in Case 2 (CBPS), loads of 105 kN to 159 kN were achieved by the stepped partially composite configurations. It was demonstrated that much of the capacity lost due to reduced shear interaction was effectively recovered by the stepped connector system. Among the fully composite beams, the CBFS model with six circle openings achieved the highest ultimate and yield loads (Fu = 166 kN, Fy = 122 kN). Whereas the six-rectangular-openings CBFS beam displayed the lowest performance (Fu = 125 kN, Fy = 88 kN), reflecting an approximation of 24% reduction attributable to sharp-corner stress concentration and impaired web stability.

Also, Table 1 showed that the trends observed in ultimate moment capacities (Mu) aligned closely with the load results, confirming the reliability of the FE predictions. For CBFS beams, i.e., fully composite configurations, Mu values ranging from 78.1 to 103.8 kN·m were recorded. Whereas values ranging from 65.6 to 99.4 kN·m were exhibited by partially composite models. The highest moment capacity was recorded for the CBFS beam with six circular openings (Mu = 103.8 kN·m), followed by the CBPS-3-stepped beam of the same configuration (Mu = 99.4 kN·m). It can be seen in this Table also that the combined effects of shear connection and opening geometry were reflected by deflection behaviour and ductility ratios. For fully composite CBFS beams, deflections at yield (δy) and ultimate deflections (δu) ranging from 10.8 to 15.2 mm and from 27.2 to 42.5 mm were recorded, respectively, yielding ductility ratios (δu/δy) of 2.52–2.80. Increased ductility was exhibited by stepped CBPS configurations, particularly in the CBPS-3 series, i.e., the 3-Stepped partially composite arrangement, where ratios of 3.44 and 3.27 were reached for the twelve-octagonal-opening beam and the six-square-opening beam, respectively. This represented a 23–36% improvement over fully composite specimens. This enhancement was attributed to the distributed shear transfer facilitated by the stepped connectors. Consequently, controlled yielding of both steel and RC components was allowed, and higher energy absorption prior to failure was achieved. Higher ductility was achieved in steel beams with circular, octagonal, and hexagonal openings compared to those with rectangular openings. The interface slip analysis further confirmed the role of shear connection detailing in composite action efficiency. CBFS beams exhibited end slips of 0.63–0.85 mm (as shown Table 1). This suggested a strong interfacial bonding and effective shear transfer. Moreover, reducing the degree of connection to η = 0.5 in CBPS beams the slip was increased to 1.78–2.45 mm. Beams with rectangular and square openings exhibited higher slip due to localized deformations and reduced cross-sectional stiffness, consistent with their lower ductility and strength.

Aca. Intl. J. E. Sci. 2026;4(1) 24-42. **DOI**: https://doi.org/10.59675/E412

Table 1: Parameters Investigated

Beam ID	**CBFS (η =1.0)**										**CBPS (η =0.5)**									
Opening Shape	**Circle**		**Octagon**		**Hexagon**		**Square**		**Rectangle**		**Circle**		**Octagon**		**Hexagon**		**Square**		**Rectangle**	
Opening Number	12	6	12	6	12	6	12	6	6	3	12	6	12	6	12	6	12	6	6	3
Failure Mode	W-P B	F	W-P B	F	F	F	V-H & W-P	F	V-H	F	W-P B	W-P B	W-P B	W-P B	W-P B	F	V-H & W-P	V-H	V-H	F
Fu (kN)	151	166	142	162	138	158	135	155	125	145	131	145	124	142	120	138	118	135	105	126
Fy (kN)	112	122	104	122	100	118	98	116	88	108	91	99	82	98	79	96	78	94	65	88
Mu (kN.m)	94.4	103.8	88.8	101.3	86.3	98.8	84.4	96.9	78.1	90.6	81.9	90.6	77.5	88.8	75	86.3	73.8	84.4	65.6	78.8
δy (mm)	12.1	10.8	13.8	11.2	14.2	11.5	14.5	11.8	15.2	12.8	13	11.2	14.5	11.8	15.2	12.2	15.8	12.6	18.5	13.5
δu (mm)	31.8	27.2	36.2	28.5	37.8	29.2	38.2	30.2	42.5	32.5	35.2	29.4	40.8	30.9	42.5	31.8	42.5	33.5	48.2	35.8
Ductility Ratio	2.63	2.52	2.62	2.54	2.66	2.54	2.63	2.56	2.8	2.54	2.71	2.63	2.81	2.62	2.8	2.61	2.69	2.66	2.61	2.65
Slip (mm)	0.73	0.63	0.75	0.66	0.78	0.68	0.78	0.69	0.85	0.72	2.08	1.78	2.18	1.86	2.25	1.92	2.28	1.98	2.45	2.15
BEAM ID	**CBPS-2-stepped (η = 0.5)**										**CBPS-3-stepped (η = 0.5)**									
Opening Shape	**Circle**		**Octagon**		**Hexagon**		**Square**		**Rectangle**		**Circle**		**Octagon**		**Hexagon**		**Square**		**Rectangle**	
Opening Number	12	6	12	6	12	6	12	6	6	3	12	6	12	6	12	6	12	6	6	3
Failure Mode	W-P B	F	W-P B	F	W-P B	F	V-H & W-P	W-P B	V-H	F	W-P B	F	W-P B	F	V-H & W-P B	F	V-H & W-P	V-H	V-H & W-P B	F
Fu (kN)	137	151	130	148	126	144	124	141	112	132	145	159	137	156	133	152	131	149	118	140
Fy (kN)	101	109	92	108	89	106	88	104	78	98	105	113	96	113	93	110	92	108	82	102
Mu (kN.m)	85.6	94.4	81.3	92.5	78.8	90	77.5	88.1	70	82.6	90.6	99.4	85.6	97.5	83.1	95	81.9	93.1	73.8	87.5
δy (mm)	12.6	10.9	14	11.4	14.8	11.8	15.2	12.2	17.8	12.9	12.3	10.6	13.6	11	14.4	11.4	14.8	11.9	16.9	12.4
δu (mm)	37.6	31.5	43.5	33.1	45.2	34.2	45.8	35.8	52.1	38.2	40.8	34.2	46.8	36.2	48.6	37.5	49.2	38.9	56.3	41.8
Ductility Ratio	2.98	2.89	3.11	2.9	3.05	2.9	3.01	2.93	2.93	2.96	3.32	3.23	3.44	3.29	3.38	3.29	3.32	3.27	3.33	3.37
Slip (mm)	1.59	1.38	1.68	1.44	1.73	1.48	1.75	1.52	1.88	1.65	1.42	1.24	1.52	1.28	1.58	1.32	1.58	1.36	1.65	1.48

Aca. Intl. J. E. Sci. 2026;4(1) 24-42. **DOI**: https://doi.org/10.59675/E412

4.1- Failure Modes and Stress Mechanisms

The FE simulations provided a detailed understanding of the progressive deformation and ultimate failure behaviour for the wide CCS composite beams. The analysis demonstrated that the overall structural response was governed by three primary mechanisms as the following stages:

- Stage I: Web-Post Buckling (W-P B) in which buckling was initiated at the opening locations.
- Stage II: Vierendeel Hinging (V-H) in which hinges were developed at the corners of the openings.
- Stage III: Flexural failure of the RC slab (F) in which the final failure mode was observed.

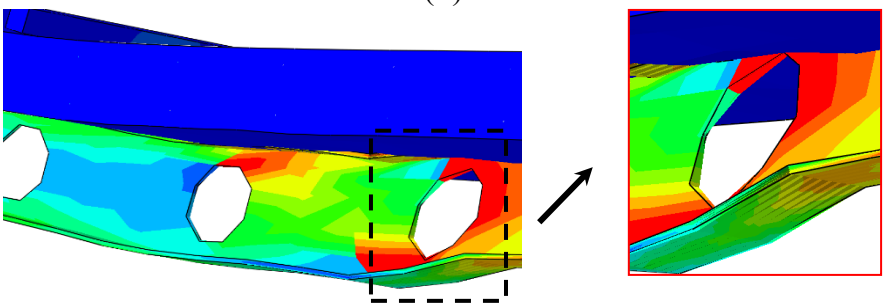

Figure 8. Web-Post Buckling (W-P B) Failure Mode of Octagon Opening –NO. 6

The dominance of these mechanisms was strongly dependent on the geometry and number of the web openings. It also depends on the degree of shear connection (η) between the steel beam and RC slab. At the early stage of loading, a uniformly stress distribution was observed in the steel web contours. This was attributed to the effective composite interaction between the steel and RC components. As the applied load was increased, stress concentrations was developed around the edges of the cellular openings. These concentrations were particularly pronounced at the narrow web-post regions separating adjacent holes. In the case of beams with circular and octagonal openings, the load-transfer paths around the opening boundaries were smooth and continuous, producing uniform stress diffusion and delaying the onset of instability. At higher load levels, localized compressive stresses formed at the mid-height of the web-posts, leading to out-of-plane deformations and eventually web-post buckling, as illustrated in Figure (8) and Figure (9) (The 6-octagonal-opening beam (CBFS) and 12-circular-opening beam are representative examples of this behaviour). The numerical simulations revealed that this buckling typically initiated near the line loads and propagated symmetrically toward the flanges.

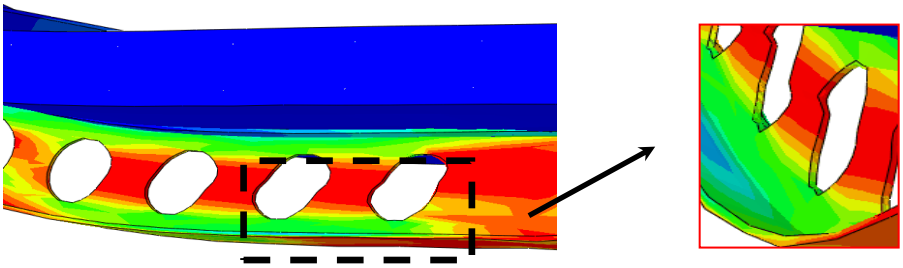

Figure 9. Web-Post Buckling (W-P B) Failure Mode of Circle Opening NO. 12

Aca. Intl. J. E. Sci. 2026;4(1) 24-42. **DOI**: https://doi.org/10.59675/E412

In contrast, a different stress distribution pattern dominated by Vierendeel hinging was exhibited by beams containing rectangular and hexagonal openings, often accompanied by secondary web-post buckling. Specifically, high stress concentrations were created around the sharp corners of the rectangular openings. As illustrated in Figure 10, Vierendeel hinge was formed in this region under increasing load. Consequently, visible distortion of the opening boundaries and the formation of diamond-shaped openings were observed.

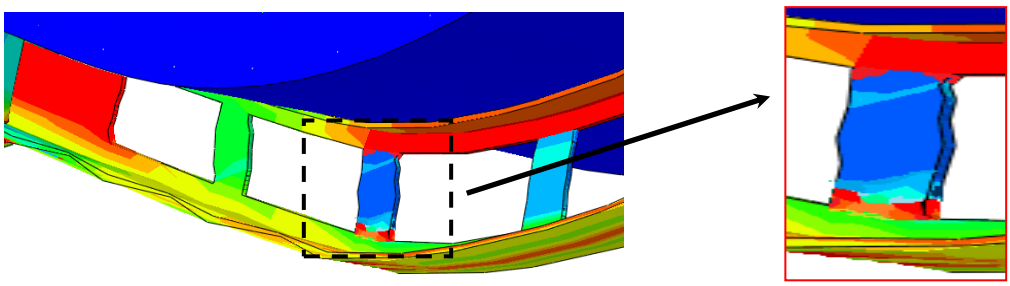

Figure 10. Vierendeel Hing & Web-Post Buckling (V-H& W-P B) Failure Mode of Rectangular Opening NO. 6

The hexagonal openings showed a somewhat improved response due to the inclined sides that distributed shear stresses more evenly; nevertheless, with an increased number of openings (twelve) as shown in Figure (11), the effective web depth was reduced, intensifying shear demands and accelerating hinge formation. The interaction between Vierendeel action and web-post buckling produced a gradual degradation of stiffness in the load–deflection curves, consistent with the progressive yielding of the web observed in the FE strain plot.

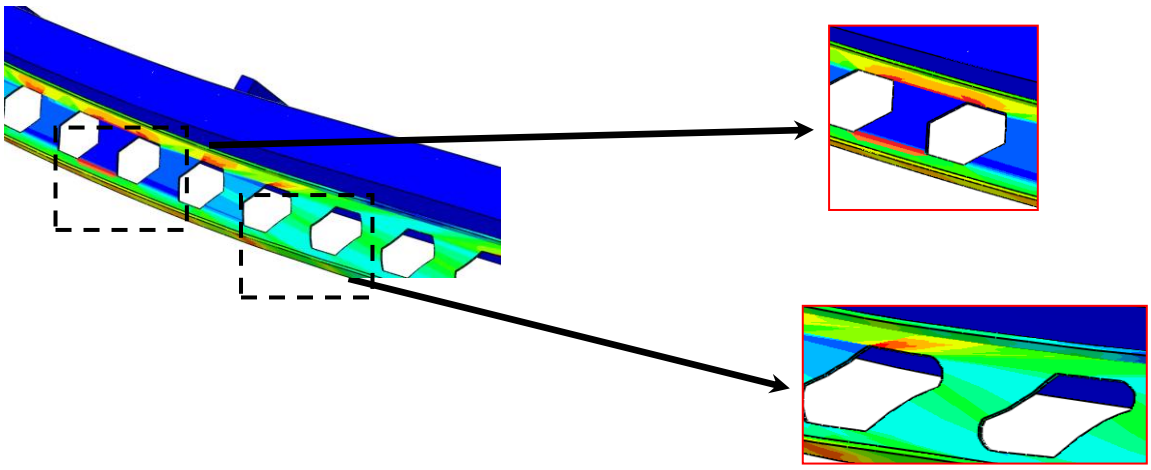

Figure 11. Vierendeel Hinge & Web-Post Buckling (V-H& W-P B) Failure Mode of Hexagon Opening NO.12

Aca. Intl. J. E. Sci. 2026;4(1) 24-42. **DOI**: https://doi.org/10.59675/E412

The flexural failure of the RC slab occurred predominantly in beams with high stiffness and strong steel webs, such as the fully composite CBFS specimens with six circular openings. In this beam, the steel section remained mostly elastic while the RC slab reached its tensile capacity at mid-span. The FE crack-pattern outputs (see Figure (12)) indicated the initiation of flexural cracks at the slab soffit, which propagated upward toward the compression zone as loading increased.

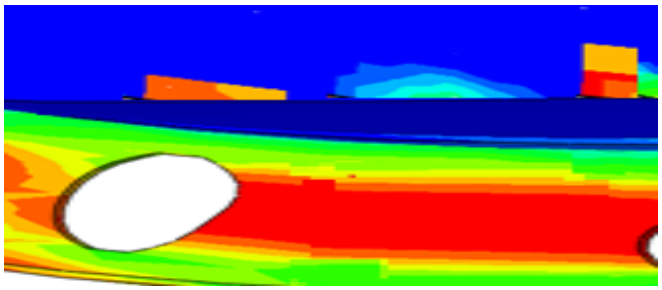

Figure 12. Flexural Failure Mode the Reinforced Concrete Slab of Circular Opening NO.6

The degree of shear connection significantly influenced the propagation of these failure mechanisms. Beams with full shear connection i.e. η=1.0 exhibited greater stiffness, improved strain compatibility, and delayed local instabilities. Conversely, partially composite beams i.e. η=0.5 developed web-post buckling at much lower loads, accompanied by wider plastic hinge zones within the web. From Figures 13, 14, and 15, it can be seen that partial connection reduced the interfacial shear transfer, allowing the steel section to deform more freely. Consequently, localized overstressing around the openings was caused.

However, when stepped shear connector configurations were introduced in the CBPS-2 and CBPS-3 models, the progression of these local instabilities was substantially delayed. The stepped arrangement improved the distribution of shear forces along the beam–slab interface, as reflected by the smoother stress gradients and smaller plastic regions in the von Mises plots (Figure (13) (14) (15)). Consequently, a more uniform strain distribution across the beam depth was achieved. Moreover, the failure mode was changed to controlled local buckling rather than unstable web collapse.

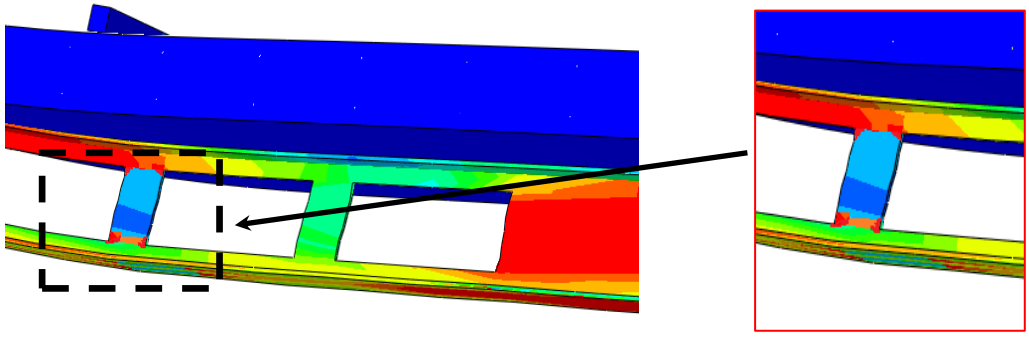

Figure 13. Vierendeel Hing (V-H) Failure Mode of Rectangular Opening NO. 6

Aca. Intl. J. E. Sci. 2026;4(1) 24-42. **DOI**: https://doi.org/10.59675/E412

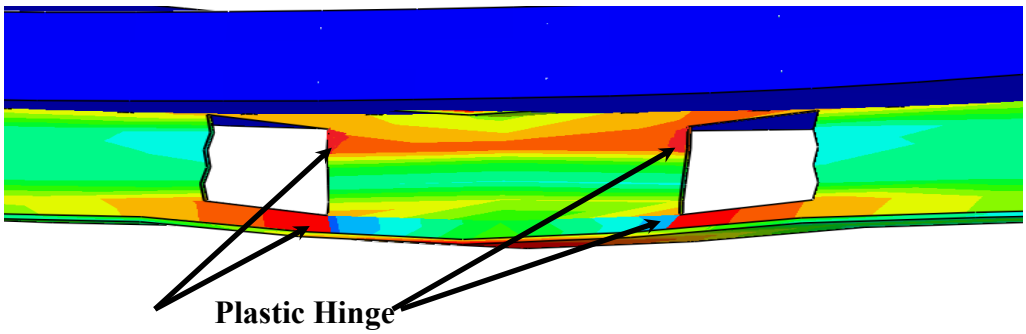

Figure 14. Vierendeel Hinge (V-H) Failure Mode of Square Opening NO.6

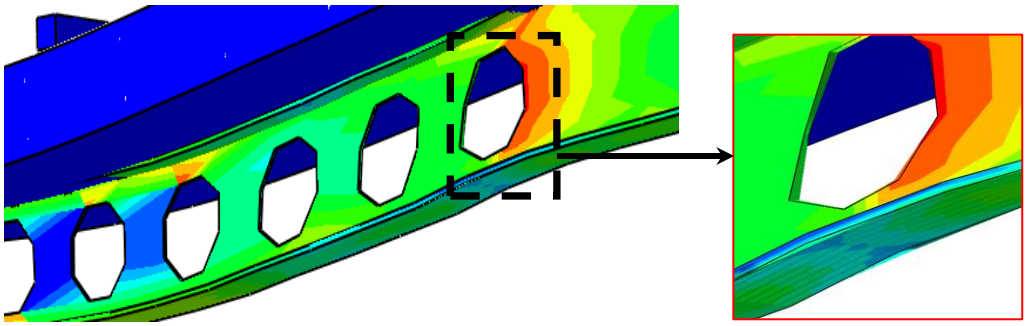

Figure 15. Web-Post Buckling (W-P B) Failure Mode of Octagon Opening NO.12

4.2- Influence of Key Parameters on Flexural Behaviour

The flexural behaviour of wide CCS composite beams is highly influenced by several design parameters, particularly the shape of the web openings, number of openings, degree of shear connection (η), and the configuration of the shear connectors. Each parameter governs the flexural load capacity, and ductility. The following discussion provides a comprehensive understanding of these parameters influence the structural response of the proposed composite beams under flexural loading.

4.2.1 Influence of Key Parameters on Flexural Load Capacity

Figure (16) showed an analysis of ultimate flexural capacity (Fu) across steel beams with various web opening shapes and different shear connector configurations of wide CCS composite beams.

Aca. Intl. J. E. Sci. 2026;4(1) 24-42. **DOI**: https://doi.org/10.59675/E412

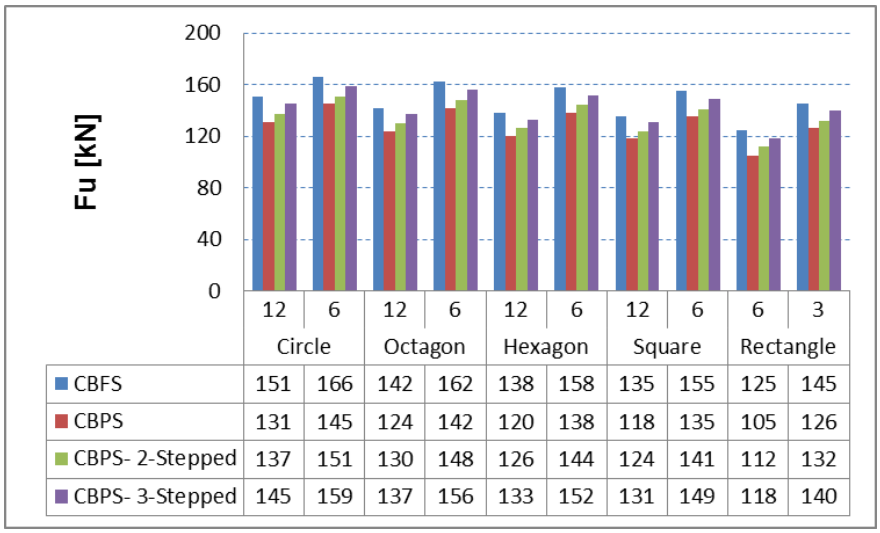

	12	6	12	6	12	6	12	6	6	3
	Circle		Octagon		Hexagon		Square		Rectangle	
CBFS	151	166	142	162	138	158	135	155	125	145
CBPS	131	145	124	142	120	138	118	135	105	126
CBPS- 2-Stepped	137	151	130	148	126	144	124	141	112	132
CBPS- 3-Stepped	145	159	137	156	133	152	131	149	118	140

Figure 16. Flexural Load Capacity of Wide Concrete–Cellular Steel Composite Beams with Various Opening Shapes and Shear Connection Configurations

The results show that composite beams with circular openings illustrate magnificence sensitivity to both openings number and shear connector configurations. The CBFS beam capacity with six opening is 166 kN, which representing the highest capacity obtained. However, this capacity reduced to 151 kN when the number of openings increases to twelve under the same full shear connection condition.

Figure 16 showed that, steel beams with hexagonal openings exhibited moderate behaviour characteristics across the range of shear connection configurations examined. An ultimate load of 158 kN was yielded by the full shear connection arrangement with six openings.

A consistent behaviour across different opening numbers was illustrated in the case square openings, with noticeably lower flexural capacities compared to circular and octagonal geometries. An ultimate load of 155 kN was achieved by the CBFS composite beam with six openings (see Figure (16)). Whereas 135 kN was reached by the CBFS composite beam with twelve openings.

In case of beams with rectangular openings, the lowest load-carrying capacity among all opening shapes were displayed, with values ranged from 105 to 145 kN. Substantial variation based on opening quantity was shown by the results, as evidenced by the difference between beams with six openings under CBPS conditions and with those having three openings under CBFS conditions, which yielded 105 kN and 145 kN, respectively. More severe stress concentrations were potentially produced by rectangular openings than other shapes.

Aca. Intl. J. E. Sci. 2026;4(1) 24-42. **DOI**: https://doi.org/10.59675/E412

4.2.2. Influence of Key Parameters on Ductility Ratios

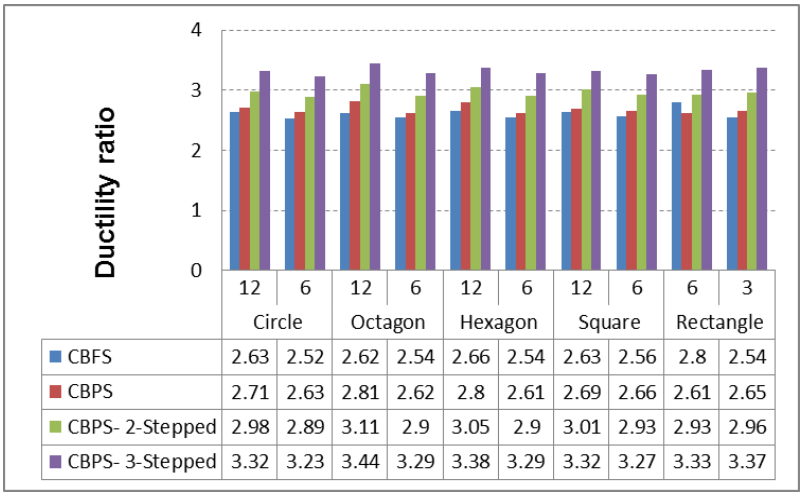

	12	6	12	6	12	6	12	6	6	3
	Circle		Octagon		Hexagon		Square		Rectangle	
CBFS	2.63	2.52	2.62	2.54	2.66	2.54	2.63	2.56	2.8	2.54
CBPS	2.71	2.63	2.81	2.62	2.8	2.61	2.69	2.66	2.61	2.65
CBPS- 2-Stepped	2.98	2.89	3.11	2.9	3.05	2.9	3.01	2.93	2.93	2.96
CBPS- 3-Stepped	3.32	3.23	3.44	3.29	3.38	3.29	3.32	3.27	3.33	3.37

Figure 17. Ductility Ratios of Wide Concrete–Cellular Steel Composite Beams with Various Opening Shapes and Shear Connection Configurations

Figure (17) illustrates the ductility ratio across steel beams with various web opening shapes (circular, octagonal, hexagonal, square, and rectangular) distributed in 3, 6, or 12 openings along the steel beam span and different shear connector configurations (CBFS, CBPS, 2-Stepped and 3-Stepped CBPS) of wide CCS composite beams.

In general, the results show that composite beams with partial shear connecters consistently exhibit more ductile compared to their fully connected counterparts. For example, The 3-Stepped CBPS configuration showed the highest ductility ratios, with data ranging from 3.23 to 3.44. This is due to that shear connector configuration facilitate more plastic deformation before failure, by promoting a more distributed yielding mechanism and postponing early connection failure.

The ductility ratios of circular opening ranging from 2.52 and 3.32 depend on shear connector configurations and opening number. For the case of steel beams with twelve circular openings, a ductility ratio of 3.32 was reached by the 3-Stepped CBPS, representing 26% improvement over the CBFS which achieved 2.63.

For the case of hexagonal openings, ductility ratios ranging from 2.54 to 3.38 were observed through the investigated key parameters.

Ductility trends for both square and rectangular opening were relatively comparable. Ductility ratios of beams with six square openings spanning from 2.56 (CBFS) to 3.27 (3-Stepped CBPS). The opening number and ductility ratio showed accurate patterns that change with connection condition. For CBFS, increasing the number of openings from three to twelve generally produces modest effects on ductility ratio, with variations within 5-10% for any given geometry. However, under partial connection condition, particularly the stepped configurations, the effects of opening number becomes more obvious

Aca. Intl. J. E. Sci. 2026;4(1) 24-42. **DOI**: https://doi.org/10.59675/E412

5. Conclusions

This research numerically investigated the effect of web opening shapes, the number of openings, and the degree and configuration of the shear connections on the performance of wide composite cellular RC beams. The following key conclusions can be drawn:

1. The bending behaviour and shear force transition of the composite beams studied in the experimental reference study (Victoire et al., 2024) were accurately predicted by a detailed numerical model.
2. Higher load-bearing capacity and ductility were exhibited by beams with circular and octagonal openings compared to those with rectangular or square openings.
3. A crucial role in governing the composite interaction, enhanced distribution of shear forces along the steel beam-RC slabs interface, and overall flexural behaviour of wide CCS beams was played by the degree of shear connection (η) between the steel beam and the RC wide beam.
4. Reduced shear transmission efficiency was resulted from partial shear bonding of the cellular steel beams, which led to premature web bending and early onset of both web post buckling and Vierendeel hinge failure.
5. It was demonstrated by the results that a desirable balance between stiffness, strength, and ductility was achieved through optimizing the shape and number of openings and the configuration of shear studs, ensuring stable and ductile performance under static loads.

Conflict of Interest

The authors declare no conflicts of interest related to this study

Acknowledgments

The authors would like to acknowledge the college dean and the head of the Civil Engineering Department in Al-Nahrain University for all help and support provided by them

References

1. Abambres M, He J. Shear capacity of headed studs in steel–concrete structures: analytical prediction via soft computing. 2019.
2. He J, Lin Z, Liu Y, Xu X, Xin H, Wang S. Shear stiffness of headed studs on structural behaviours of steel–concrete composite girders. Steel Compos Struct. 2020; 36:553–568.
3. Zhang F, Wang C, Zou X, Wei Y, Chen D, Wang Q, Wang L. Prediction of the shear resistance of headed studs embedded in precast steel–concrete structures based on an interpretable machine learning method. Buildings. 2023;13:496.
4. Meng H, Wang W, Xu R. Analytical model for the load–slip behaviour of headed stud shear connectors. Eng Struct. 2022;252:113631.
5. Guang C. Shear capacity evaluation of studs in steel–high strength concrete composite structures. Appl Eng Sci. 2024;17:100150.
6. Mia MM, Bhowmick AK. Static strength of headed shear stud connectors using FE analysis. In: Proceedings of the 6th International Conference on Engineering Mechanics and Materials; 2017; Vancouver, BC, Canada. Vol 31.
7. Wang S, Fang Z, Chen G, Jiang H, Teng S. Numerical analysis on shear behaviour of grouped head stud shear connectors between steel girders and precast concrete slabs with high-strength concrete-filled shear pockets. J Bridge Eng. 2021;26:04021030.

8. Ernst S. Factors affecting the behaviour of the shear connection of steel–concrete composite beams [PhD thesis]. Sydney (Australia): University of Western Sydney; 2006.
9. Baran E, Topkaya C. Behaviour of steel–concrete partially composite beams with channel-type shear connectors. J Constr Steel Res. 2014;97:69–78.
10. Henderson IEJ, Uy B, Zhu XQ, Mirza O. The effect of retrofitted shear connection systems on the dynamic response of composite concrete–steel beams. In: Australasian Conference on the Mechanics of Structures and Materials; 2014; Southern Cross University. p. 639–644.
11. Pardeshi RT, Patil YD. Review of various shear connectors in composite structures. Adv Steel Constr. 2021;17:394–402.
12. Xue C, Fan Z, Wu F, Liu L, He L, Cui X. Research on the shear behaviour of composite shear connectors. Buildings. 2022;12:1726.
13. Shahabi S, Sulong N, Shariati M, Shah S. Performance of shear connectors at elevated temperatures: a review. Steel Compos Struct. 2016;20:185–203.
14. Ding Y, Wang XD, Shen MH, Chung KF, Zhou XH, Elghazouli AY. Deformation characteristics of ductile large-resistance shear connections for practical composite beams. Eng Struct. 2024;320:118838.
15. Anbu HK, Kothandapani K. Enhancing structural reusability and durability: a review of steel–concrete shear connector systems in modular construction. Adv Sci Technol Res J. 2025;19:70–97.
16. Wang M. Structural performance of a novel sustainable and demountable composite floor system—recycled aggregate concrete–steel composite beam utilising demountable shear connectors [Doctoral thesis]. Glasgow (UK): University of Glasgow; 2025.
17. Suba Sreenidhi G, Senthil Kumar G. Demountable shear connector in steel–concrete composite floors: a state-of-the-art review. In: International Conference on Civil Engineering Innovative Development in Engineering Advances; 2023; Singapore. p. 373–381.
18. Qi J, Wang J, Li M, Chen L. Shear capacity of stud shear connectors with initial damage: experiment, FEM model and theoretical formulation. Steel Compos Struct. 2017;25:79–92.
19. Tu X, Wu Y. Numerical analysis on corrosion and mechanical performance of shear stud connectors in concrete. Constr Build Mater. 2023;363:129816.
20. Ma S, Lou Y, Bao P. Experimental research and numerical analysis of shearing resistance in steel–concrete composite beam connectors. Case Stud Constr Mater. 2022;17:e01210.
21. Xue C, Huang H, Jia Q. Shear mechanism of a novel SFCBs-reinforced composite shear connector: experimental, theoretical investigations and numerical model. Materials. 2024;17:3508.
22. Yan Q, Chen X, Jia B, Yu X, Zheng Y, Chen Z. Theoretical and FEA study on shear performance of novel shear connectors. J Constr Steel Res. 2025;225:109186.
23. Mansur MA, Tan KH. Concrete beams with openings: analysis and design. 3rd ed. Boca Raton (FL): CRC Press; 1999. p. 1–400.
24. Sunar Bükülmez P, Celik OC. Experimental study on fire behaviour of steel–concrete composite cellular beams with large opening ratio. Int J Steel Struct. 2020;20:207–231.
25. Dong Y, Jia L, Xu F, Li X. Experimental study on seismic behaviour of steel structures with cellular beams and composite concrete slabs. In: Structures. Amsterdam: Elsevier; 2021. Vol 34. p. 507–522.
26. Victoire AB, Mwero JN, Gathimba N. Experimental study on the effect of partial shear stud layout on flexural behaviour of steel–concrete composite beams. Results Eng. 2024;21:101959.